A Mixed Finite-Element Treatment of Rotor Blade Elongation

Gene C. Ruzicka
Aerospace Engineer
Army/NASA Rotorcraft Division
Aeroflightdynamics Directorate (AMRDEC)
U.S. Army Aviation and Missile Command
Ames Research Center
Moffett Field, California

Dewey H. Hodges
Professor
School of Aerospace Engineering
Georgia Institute of Technology
Atlanta, Georgia

Abstract

The accuracy of rotor blade basis reduction hinges critically on how axial elongation is treated. This fact is illustrated by analyzing an articulated rotorcraft blade using several blade formulations, and comparing their basis reduction accuracies. It is shown that classical, displacement-based finite elements fail to accurately represent the blade's axial strain when the blade's basis is reduced because of ill conditioning caused by the near inextensibility of the blade. This problem may be solved by introducing the axial force, or a related quantity, as a variable in the analysis. The mixed finite-element method is the preferred approach for accomplishing this because it imposes no restrictions on the model's geometry, but it leads to additional degrees of freedom and does not explicitly account for the nonlinear axial foreshortening effect. It is shown how both of these shortcomings may be removed by using the mixed element force equations to eliminate axial displacement degress of freedom in favor of axial force and bending degrees of freedom. The elimination process is formulated first for a single element, and then for an arbitrary assemblage of elements. In essence, the procedure may be viewed as a generalization, to blades of arbitrary geometry, of the axial elongation variable, which is widely used by rotorcraft analysts.

Introduction

The application of the finite-element method to rotorcraft analysis over the past two decades has removed the topological restrictions on the models that can be analyzed using older, first-generation rotorcraft codes. Although full finite-element models may be preferred for final analyses for reasons of accuracy and reliability, it is often convenient in earlier stages of the analysis to reduce the size of the model to a small number of generalized coordinates to improve execution time or to assist in interpreting and understanding the results. The basis reduction process is typically accomplished via the *modal reduction* method, which employs eigenmodes computed about some convenient state. Unfortunately, it is often quite difficult to approximate blade response accurately using just a few eigenmodes when the axial motion is parameterized using the Lagrangian axial displacement variable. The reason is that the near inextensibility of the blade nonlinearly couples the blade's axial and bending motions and ill conditions the calculation of the blade's axial force. As a result, the blade's axial displacement, and more importantly, the blade's axial force, may not be computed accurately. But since the blade's bending stiffness is mostly geometric stiffness generated by the axial force, incorrectly evaluating that quantity can lead to significant errors in blade response.

The computational problems caused by the axial displacement variable have long been recognized. The most common remedy for these problems has been a change of variable, which parameterizes the axial displacement field with an

Presented at the American Helicopter Society Aeromechanics Specialists' Meeting, Atlanta, Georgia, November 13-15, 2000.

axial elongation variable instead of the usual *axial displacement* variable. This variable is defined in terms of an integral of the elongation of the reference line, but since the integrand cannot be obtained as the derivative of some quantity, the variable may be viewed as a *quasi-coordinate* (analogous to the characterization of the integrals of certain velocity variables in dynamics.) The approach goes back at least to Vigneron in the 1970's (Refs. 1, 2) and has been considered by numerous other investigations since then; see, for example, Refs. 3, 4, 5. Although the effectiveness of this approach for modal expansion methods has been well documented, its inherently one-dimensional framework may limit the structural geometries that it can be applied to. Also, the integral can complicate finite-element analyses by causing a given degree of freedom to become explicitly coupled through the inertia terms to degrees of freedom at locations further inboard. These undesriable features have spurred the search for alternative approaches. However, Smith (Ref. 6) showed that modal reduction of a finite-element model could be facilitated by this change of variable.

Mixed finite elements, hereafter abbreviated as "mixed elements," have been proposed for rotor blade analysis by Hodges (Ref. 7). and by Bauchau and Guernsey (Ref. 8). In Ref. 8, the modal reduction accuracy of mixed elements was studied, but disappointing results were obtained, especially for torsional response, even when the mixed elements were supplemented by perturbation modes, Ref. 9. But more recently, the authors' work, Refs. 10 and 11, demonstrated generally good modal reduction accuracy for all blade motions, including torsion, when mixed elements were used to model an articulated rotor blade. It should be noted that the only mixed aspect of the authors' work is related to the axial displacement field. Still another approach to basis reduction is the "nonlinear normal mode" method presented in Refs. 12 and 13, which replaces the classical eigenmode, with its fixed relationships among the degrees of freedom, with a nonlinear set of functions termed an "invariant manifold," which is extracted from the governing equations. Interestingly, all these approaches, including the one developed in this paper, can be shown to be fundamentally related (Ref. 14), although there are significant differences in how they are implemented and in the types of models they can treat.

Although the mixed finite-element method appears adequate for comprehensive rotorcraft analysis in its current form, it is noted that the method can withstand further refinement in two respects: first, the blade axial response is not approximated quite as well as the other responses; and, in addition, it is desirable to eliminate additional generalized coordinates that must be introduced into the modal reduction scheme to preserve the independence of the axial force and axial displacement generalized coordinates in modal space (see Ref. 11). Introducing these refinements into the mixed finite-element rotor blade analysis that was presented in Ref. 11 is the first goal of this paper. An additional, broader aim of this paper is to lay the groundwork for broadening the method into a truly global procedure for analyzing axial foreshortening effects that can be applied to models containing arbitrary assemblages of two and three dimensional elements as well as beam elements.

In what follows, a rationale for the use of mixed elements is developed starting from the Hodges-Dowell equations (Ref. 15) of a rotor blade specialized to axial and flap motions. The derivation of a mixed element is then described, and the element's effectiveness in modal reduction is illustrated by using it in the analysis of an articulated blade model. Then, the mixed finite element is revised by employing the axial force equations to eliminate the Lagrangian axial displacement degrees of freedom in favor of axial force degrees of freedom for the case of a single element. The single element analysis is extended to an arbitrary assemblage of beam elements through suitably generalizing the axial displacement concept, and then developing a procedure that solves for the generalized axial displacement degrees of freedom in terms of bending and axial force degrees of freedom. This procedure effectively generalizes the axial elongation variable concept to blades of arbitrary geometry. Finally, there is a discussion of the applicability of the procedure to models containing structural components other than beams.

It is to be emphasized that the focus of this paper is on the adequacy of modal reduction methods rather than on validating the rotor blade analyses. However, the analysis examples presented here embody many of the key features rotor blades and their loadings under flight conditions, and it is therefore felt that the modal reduction accuracies demonstrated here will be typical of actual rotor blades.

Rationale for Mixed Elements

Preliminaries: Hodges-Dowell flap-axial blade equations

The discussion starts with the Hodges-Dowell blade equations (Ref. 15) specialized to coupled axial-flap motions:

$$V_x' = -m\Omega^2 x - f_x \tag{1}$$
$$m\ddot{w} = (V_x w')' - (EI_y w'')'' + f_z \tag{2}$$

where V_x is the axial force, m is the mass per unit length, x is the axial coordinate, Ω is the rotor angular speed, w is the flap displacement, EI_y is the cross section flap flexural rigidity, and f_x and f_z are applied forces per unit length. Following the usual conventions in the rotorcraft literature, $(\,)'$ denotes partial differentiation with respect to the axial coordinate, and $\dot{(\,)}$ denotes partial differentiation with respect to time. If the blade is clamped at the spin axis, the boundary conditions are:

$$w|_{x=0} = w'|_{x=0} = 0 \tag{3}$$

These equations are particularly useful for examining blade analysis methods because they are simple enough to permit easy inspection, yet they embody the key axial stiffening and axial foreshortening phenomena.

In what follows, various mathematical formulations for rotor blade analysis are presented, culminating with a mixed element. The formulations, which differ primarily in how they treat axial displacement and axial elongation, are evaluated based on their modal reduction accuracy, and the key features of the mixed element are introduced in a step-by-step fashion.

Method 1: the axial displacement variable

This method represents all variables in terms of displacement fields, and then applies polynomial discretization of the fields over sub-regions of the model, which are simply finite elements. The following expression for axial force is used, which is consistent with the Hodges-Dowell ordering scheme:

$$V_x = EA\left(u' + \frac{1}{2}w'^2\right) \tag{4}$$

where EA is the axial stiffness of the blade cross section. Substituting equation (4) into the Hodges-Dowell equations, and then reintroducing the (formally negligible) contributions of u and $\ddot{u}$ into the axial acceleration gives:

$$m\ddot{u} = \left[EA\left(u' + \frac{1}{2}w'^2\right)\right]' + m\Omega^2(x+u) + f_x \tag{5}$$
$$m\ddot{w} = \left[EA\left(u' + \frac{1}{2}w'^2\right)w'\right]' - (EI_y w'')'' + f_z \tag{6}$$

where $m\ddot{u}$ and $m\Omega^2 u$ are ignored in the original Hodges-Dowell equations, but are required when the axial displacement variable is introduced. The boundary conditions for a blade clamped at the spin axis are

$$u|_{x=0} = w|_{x=0} = w'|_{x=0} = 0 \tag{7}$$

Equations (5) and (6) allow for full discretization of the blade model in the axial direction, thereby permitting the full power of the finite-element method to be brought to bear on the analysis. Unfortunately, a high price for this flexibility stems from the difficulty of approximating the axial force, which is critical for accurately computing the blade bending stiffness. The source of the difficulty is that the near inextensibility of the blade effectively ill conditions the calculation of the axial strain whenever the displacements become sizable; i.e., $\epsilon_x = \frac{V_x}{EA} = u' + \frac{1}{2}w'^2$ and therefore $|\epsilon_x| \ll |u'|$,

Node	Displacements	Forces[a]
1	u_1, v_1, v_1', w_1, w_1', ϕ_1	V_{x_1}
2	u_2, v_2, v_2', w_2, w_2', ϕ_2	V_{x_2}
Internal Degrees of Freedom	u_3, u_4, ϕ_3	V_{x_3}

[a]Force degrees of freedom appear only in the mixed element

Table 1: Beam finite element degrees of freedom.

$|\epsilon_x| \ll w'^2$ since $EA \gg 1$. As a consequence, calculating ϵ_x accurately requires far more accuracy in both u' and w'^2 than can be obtained by representing either of these quantities using a small number of eigenmodes.

The effects of the ill-conditioned axial strain computation will now be illustrated with several computational examples that employ the blade model shown in Figure 1, which is based on the properties of the UH-60 rotorcraft blade. Each element is formulated as the displacement-based aeroelastic beam element described in Ref. 16. This element

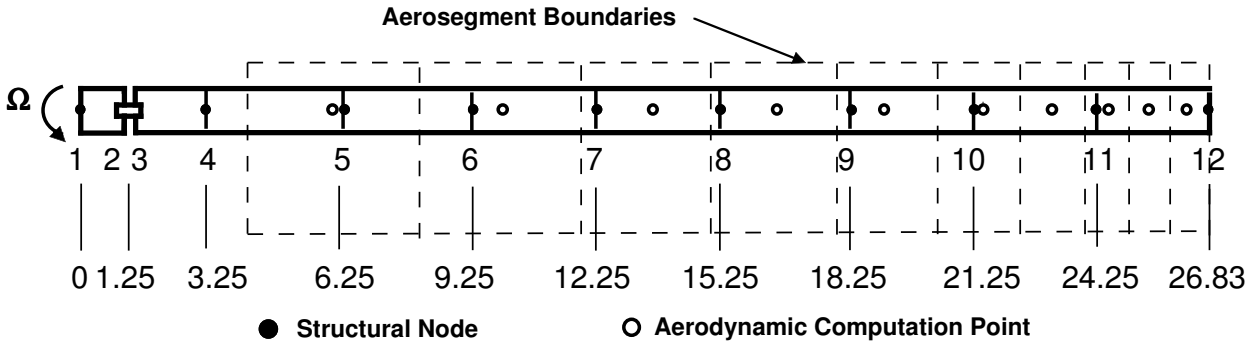

Structural Properties	Aerodynamic Properties	Flight Conditions
Radius - 26.83 ft. EI_y - 1.85E5 lb-ft^2 EI_z - 4.18E5 lb-ft^2 GJ - 2.08E5 lb-ft^2 EA - 6.69E8 lb 92 DOF's	SC1095 Airfoil Uniform Inflow Greenberg Aerodynamics Chord - 1.7405 ft	Ω=258 rev/minute θ_O=10.0 deg. θ_C=2.0 deg. θs=-7.0 deg. Θ=4.0 deg. Ψ=Φ=0.0 deg. μ=.373, C_T/σ=.072

Figure 1: UH-60 blade model.

is a displacement-only analogue of the mixed element described in Ref. 11, the only difference being that the mixed treatment applied to the axial motions in Ref. 11 is absent, but the kinematics, the interpolation functions, and the inertia forces are treated identically in both elements. The element's degrees of freedom correspond to the default configuration described in Ref. 11 (see also Ref. 17): the lag (v) and flap (w) displacements are interpolated using the standard cubic Hermitian polynomials for beam finite elements, the axial (u) displacements are interpolated using C^0 Jacobi polynomials up to third-order, and the pitch rotations (ϕ) are interpolated using C^0 Jacobi polynomials up to second-order. These interpolations result in the element having the degrees of freedom listed in Table 1.

In all computational examples, the blade response is expanded modally about the steady-state *in vacuo* spin condition, *viz.*,

$$\{q\} = \{q_{ss}\} + [\Phi]\{q_{modal}\} \tag{8}$$

where $\{q\}$ is the total blade response, $\{q_{ss}\}$ is the static response of the blade to steady-state spin, $[\Phi]$ is a column matrix of eigenmodes, and $\{q_{modal}\}$ is a vector of modal generalized coordinates.

Consider, first, an eigenanalysis of the spinning blade. The analysis assumes *in vacuo* conditions along with zero applied blade pitch. The eigenmodes are computed about deflection configurations caused by tip flap loads that result in coning angles of 4° (2539.6 lb.) and 8° (5079.2 lb.). The modal basis contains the first two flap nodes, and the number of axial modes is varied from one to thirty; note that thirty is the dimension of the axial motion subspace. The flap frequencies are plotted against the number of axial modes in Figure 2. While reasonable results are obtained for

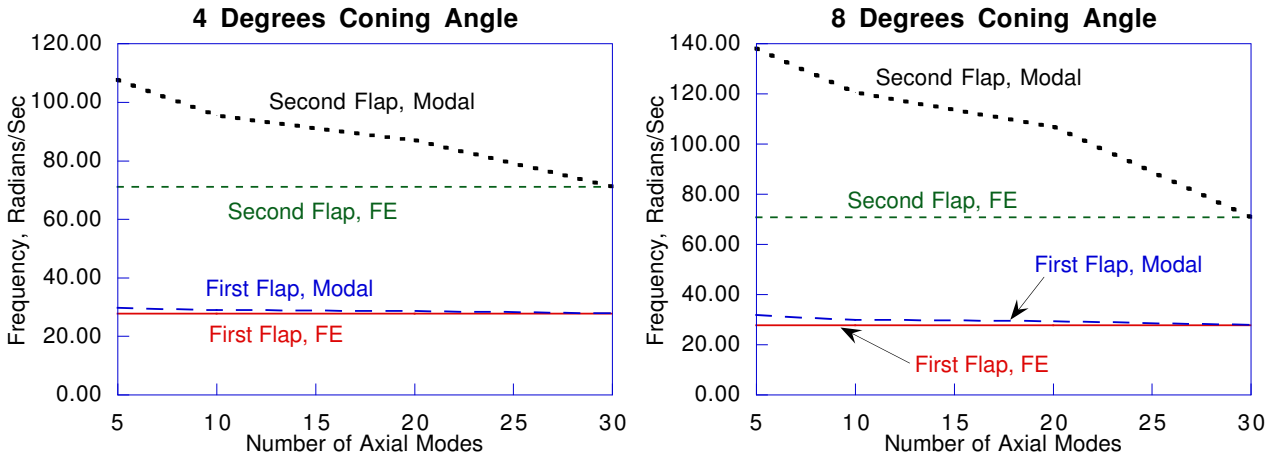

Figure 2: UH-60 blade flap frequencies: displacement elements.

the first flap frequency with just a few axial modes, the accuracy of the second flap frequency is much poorer, and does not become acceptable until almost the entire axial subspace is filled.

Consider, now, the periodic solution of the model shown in Figure 1. The *in vacuo* eigenmodes of this model are given in Table 2, and the modal bases used in the calculations are given in Table 3. In this example, all blade motions (i.e.,

Mode ID	Frequency (/rev)
First Lag	0.27
First Flap	1.03
Second Flap	2.63
Second Lag	4.09
First Torsion	4.86
Second Torsion	14.59
First Axial	22.12
Second Axial	66.41

Table 2: UH-60 blade modes.

Modal Basis	Number of Modes			
	Lag	Flap	Torsion	Axial
1l,1f,1t,1a	1	1	1	1
2l,2f,2t,2a	2	2	2	2

Table 3: Description of modal bases.

axial, flap, lead-lag, and torsion), are considered. Periodic solutions for the degrees of freedom at the tip node are

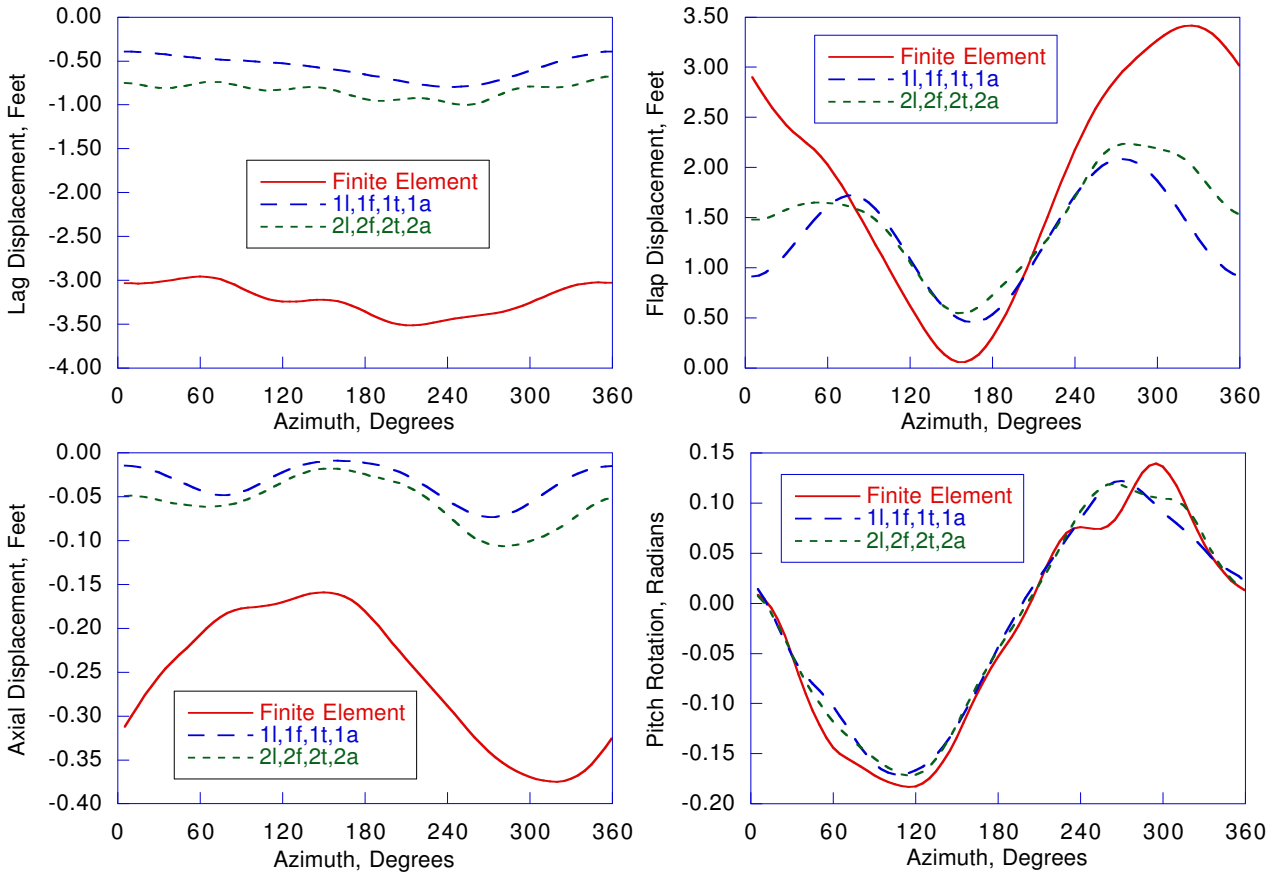

Figure 3: UH-60 blade tip deflections: displacement elements.

shown in Figure 3. The flight conditions for the analysis are given in Figure 1: θ_0, θ_c, and θ_s, are the collective, lateral cyclic, and longitudinal cyclic swashplate controls; Θ, Ψ, and Φ are the pitch, yaw and roll angles of the vehicle; $\mu = V\cos\alpha/\Omega R$ is the rotor advance ratio, where V is the vehicle speed, α is the rotor angle of attack and R is the rotor radius; $C_T = T/\rho A(\Omega R)^2$ is the thrust coefficient, where T is the rotor thrust, and A is the rotor disk area; and $\sigma = Nc/\pi R$ is the rotor solidity, where N is the number of blades, and c is the blade chord.

It may be seen that the agreement between the modal and finite-element solutions is quite poor for the flap, lag and axial displacements, as was expected. But surprisingly, the agreement between the finite-element and modal solutions is quite good for the pitch rotation. The reasons for the good modal approximations are the high torsional stiffness of the blade, combined with the low degree of bending-torsion coupling in stiff, articulated blades of the type analyzed here, although aerodynamic coupling between the torsion and bending equations is appreciable for all rotor blades. Thus, it may be inferred that the poor modal reduction accuracy of the bending response can come only from errors in solving the rotor blade bending equations.

Method 2: the axial force variable

One approach to facilitating modal reduction involves parameterizing the axial motion using the axial force rather than the axial displacement. The axial displacement may be written in terms of the axial force using equation (4):

$$u' = \frac{V_x}{EA} - \frac{1}{2}w'^2 \tag{9}$$

or

$$u = \int_0^x \left(\frac{V_x}{EA} - \frac{1}{2} w'^2 \right) ds \tag{10}$$

With this re-parameterization, the axial force is now expressed as a single variable, and the numerical conditioning problems associated with the axial displacement variable are absent.

The likely effectiveness of the axial force variable in modal reduction may be inferred from its similarity to the axial elongation variable, which is defined as:

$$u_e = \int_0^x \frac{V_x}{EA} ds \tag{11}$$

and for which the modal reduction effectiveness has been well demonstrated. Unfortunately, the approach is developed from a one-dimensional conception of the displacement field, and applying it to two-dimensional components such as plates and shells appears to be problematic. The methods that will be described subsequently in this paper are largely motivated by the desire to circumvent this restriction.

Method 3: axial force *and* axial displacement variables – a mixed element

It has been shown that parameterizing axial motions using the Lagrangian axial displacement gives unrestricted modeling freedom at the expense of ill-conditioned and highly nonlinear axial-bending coupling, while using the axial force as a variable makes modeling more awkward, but simplifies axial-bending coupling. In an attempt to obtain the advantages of both methods – without their limitations – both the axial displacement *and* the axial force will be employed as variables. This may be accomplished by augmenting the Hodges-Dowell equations with an equation that relates the axial force and the axial displacement. Three equations result:

$$\frac{V_x}{EA} = u' + \frac{1}{2} w'^2 \tag{12}$$

$$m\ddot{u} = V_x' + m\Omega^2 (x + u) + f_x \tag{13}$$

$$m\ddot{w} = \left(V_x w' \right)' + f_z \tag{14}$$

Since the axial force *and* displacements are variables in these equations, it is dubbed a *mixed element*.

The advantages of the mixed-element equations are more readily appreciated when they are expressed in variational form. That process involves applying finite-element interpolations to the three independent variables: $V_x = [H_{V_x}]\{q_{V_x}\}$, $u = [H_u]\{q_u\}$, and $w = [H_w]\{q_w\}$. In what follows, all variables are assumed to have been discretized, but – when possible – they are displayed as continuous for improved readability. Substituting the finite-element interpolations into equations (12), (13), and (14), then multiplying those equations by δV_x, δu, and δw, respectively, and finally summing the results of these operations and integrating over the length of the element gives:

$$\int_0^l (\{\delta q_{V_x}\}^T \{\bar{Y}_{V_x}\} + \{\delta q_u\}^T \{\bar{Y}_u\} + \{\delta q_w\}^T \{\bar{Y}_w\}) dx = 0 \tag{15}$$

where:

$$\{\bar{Y}_{V_x}\} = [H_{V_x}]^T \left(\frac{V_x}{EA} - u' - \frac{1}{2} w'^2 \right) \tag{16}$$

$$\{\bar{Y}_u\} = [H_u]^T [m\ddot{u} - V_x' - m\Omega^2 (x + u) - f_x] \tag{17}$$

$$\{\bar{Y}_w\} = [H_w]^T \left[m\ddot{w} - (V_x w')' - f_z \right] \tag{18}$$

For future reference, note that it is often convenient to express the discretized form of u' as follows:

$$u' = \left[H_u' \right] \{q_u\} = \left[H_{u'} \right] \{q_{u'}\} \tag{19}$$

for some set of unknowns, $\{q_{u'}\}$, which is of size $N_u - 1$.

The usefulness of the mixed element may be inferred from arguments similar to those used in discussing the axial force variable. First, consider the $\{\delta q_u\}$ variation. Setting the coefficient of that variation to zero gives, after removing the small contributions from u, and $\ddot{u}$:

$$\int_0^l [H_u]^T [V_x' - m\Omega^2 x - f_x] dx = 0 \tag{20}$$

which is analogous to the first of the Hodges-Dowell equations, and which largely determines V_x. Thus, in contrast to the axial displacement variable method, the axial force, which is a key quantity, is determined directly from what is essentially an equilibrium equation. Using V_x in the $\{\delta q_w\}$ variation gives:

$$\int_0^l [H_w]^T \left[m\ddot{w} - (V_x w')' - f_z \right] dx = 0 \tag{21}$$

which is analogous to the second of the Hodges-Dowell equations, and which largely determines w. Finally, the $\{\delta q_{V_x}\}$ variation leads to:

$$\int_0^l [H_{V_x}]^T \left(\frac{V_x}{EA} - u' - \frac{1}{2} w'^2 \right) dx = 0 \tag{22}$$

which is analogous to equation (10), and which largely determines u. Observe that *weak enforcement* of the governing equations is crucial in allowing the axial force to be computed as a separate variable. Also, weak enforcement of the force-displacement equation (equation 22) permits the implicit determination of u from that equation and eliminates the potential need to constrain the model's topology to explicitly calculate u by integrating outward from the spin axis as in equation (10).

Aside from the *analysis* advantages just described, a unique *modeling* advantage of the mixed finite-element method is that it imposes no geometric restrictions whatsoever on the model. As in displacement-based finite-element methods, Lagrangian displacements are the only variables defined at nodes where elements join. Displacements are transformed from the model level to the element level using mapping tables that relate element and model coordinate systems; conversely, forces are assembled from the element level to the model level using the transpose of the mapping table matrix. Axial force degrees of freedom are defined only within elements, not at nodes, and equilibrium equations where elements join at nodes are formed automatically by the process just described. This highly general model assembly process is identical to that used in the well known, general purpose finite-element codes, and as in those codes, it permits the construction of highly intricate finite-element models that can incorporate plate and shell elements as well as beam elements.

The mixed element equations just presented (i.e., equations 15 – 18), were developed in a rather *ad hoc* manner, and apply only to a blade with coupled axial and flap motions. In Ref. 11, a complete mixed finite element for rotor blade applications, in which coupled axial, flap, lag, and torsional motions are present, is systematically derived from a mixed variational principle. The accuracy of that element will now be illustrated using the examples considered earlier. The additional axial force degrees of freedom are interpolated using Jacobi polynomials up to second order (see Table 1, Ref. 17.) The first example is an eigenanalysis of the UH-60 blade. Plots of the first two flap frequencies versus the number of axial modes are shown in Figure 4. In contrast to the corresponding results seen in Figure 2 for the displacement element, only a single axial mode – but actually, two generalized coordinates – are required to match the finite-element results accurately.

Periodic solutions for finite-element and modal bases are compared in Figure 5 for blade tip displacements, and in Figure 6 for blade root loads. It may be seen that there is a dramatic improvement in how the modal solutions approximate blade tip displacements when compared with the corresponding results for the displacement elements (Figure 3). The axial displacement is not approximated quite as well as the other displacements, probably because of the nonlinearity of the axial foreshortening effect. However, the primary interest in the axial displacement is its impact on lag moments through the Coriolis effect, but as may be seen in Figure 6, the root lag moments are approximated quite well, which suggests that the axial displacement is sufficiently accurate for most practical purposes. Still, it is

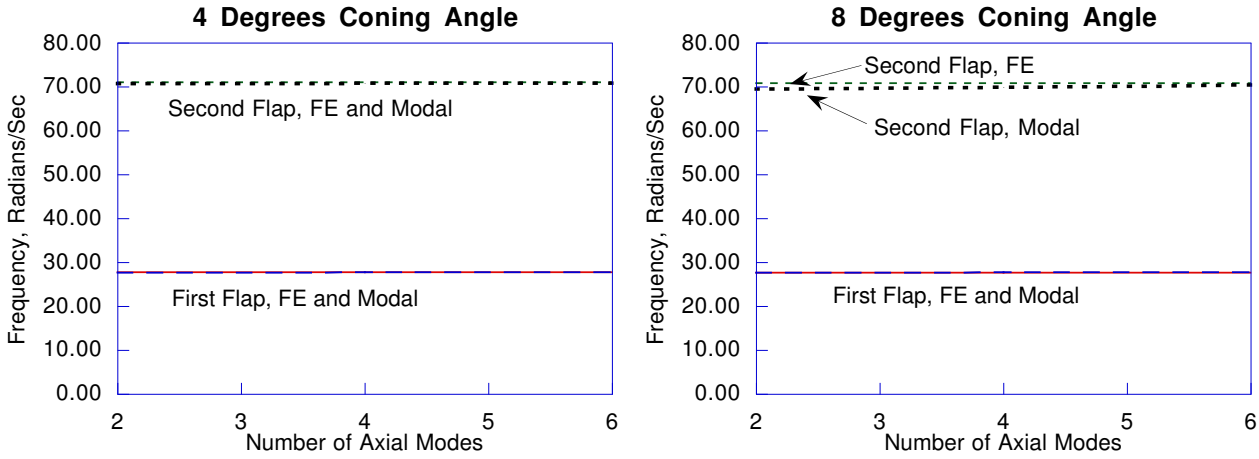

Figure 4: UH-60 blade flap frequencies: mixed elements.

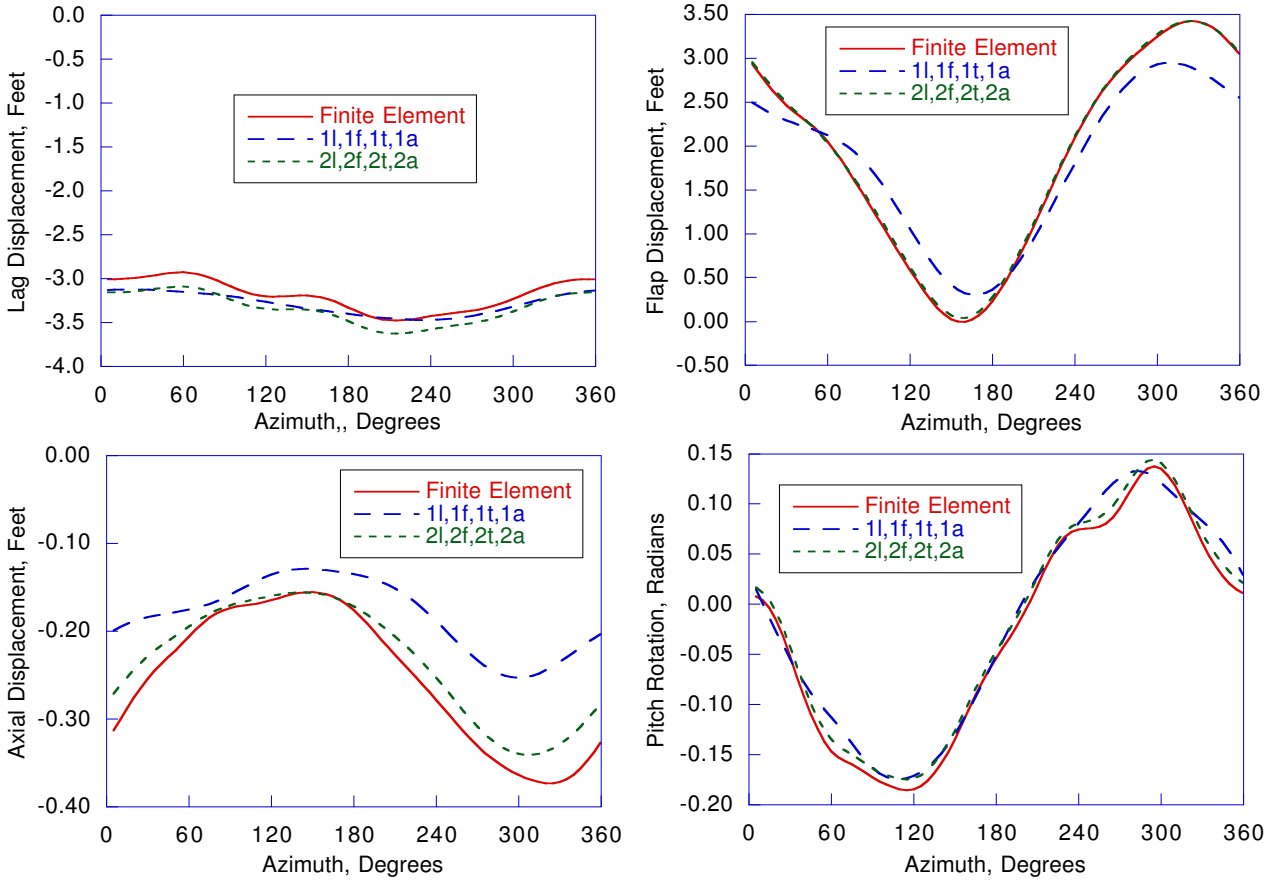

Figure 5: UH-60 blade tip deflections: mixed elements.

desirable to improve the modal approximation of the axial displacement, and a technique for doing that is the subject of the remainder of this paper.

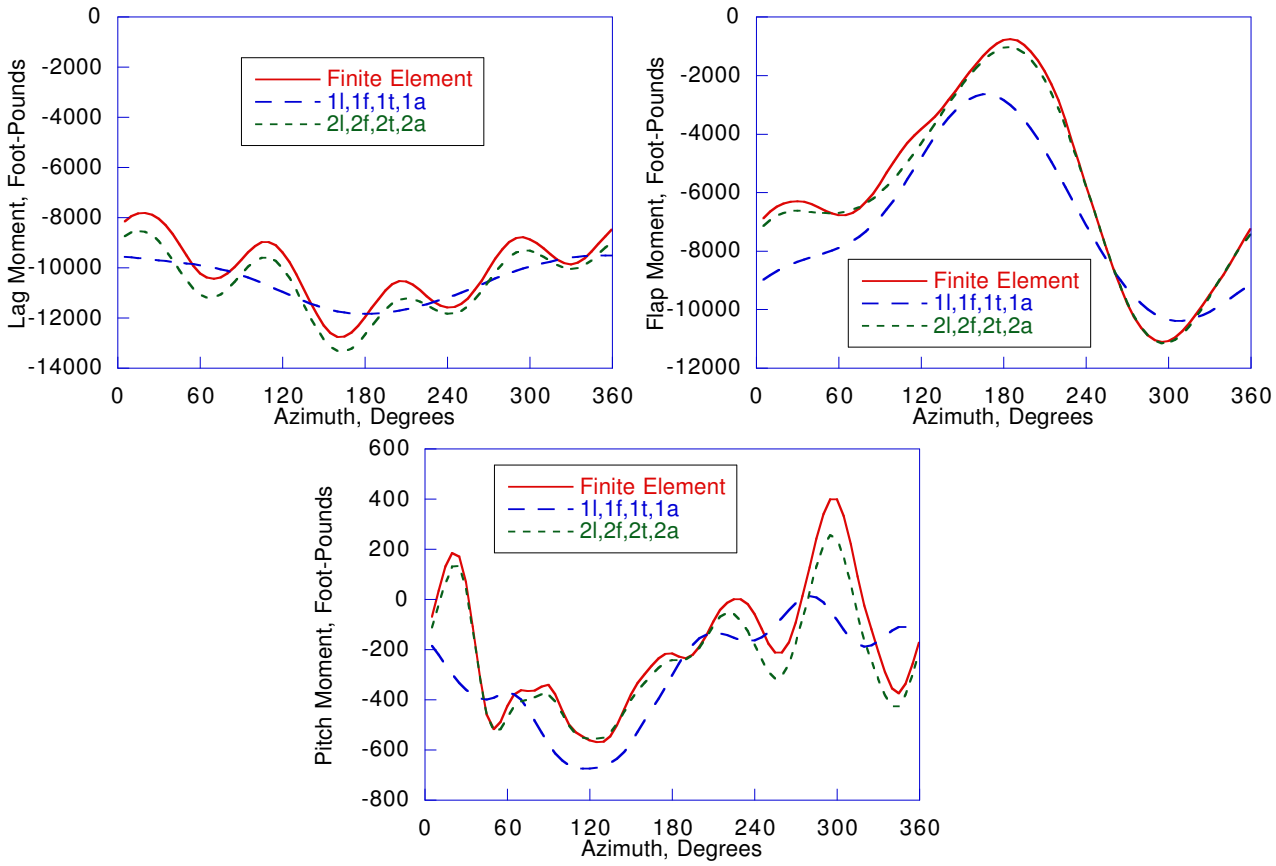

Figure 6: UH-60 blade root loads: mixed elements

Mixed Finite-Element Analysis of Axial Displacements

Overview

An interesting feature of the axial force variable method becomes apparent upon examination of equation (10). As noted earlier, the axial strain is significantly smaller than the deformation gradient quantities and, if that term is dropped, there results:

$$u = -\int_0^x \frac{1}{2} w'^2 ds \tag{23}$$

which is the axial foreshortening term. In other words, the axial foreshortening effect is embedded within the axial force variable method. The mixed finite-element analogue of equation (10) is equation (22), which does not approximate the foreshortening effect well in modal space because the axial displacement is obtained by a *linear* superposition of eigenmodes. However, it seems that if – analogous to equation (10) – one were to solve equation (22) for the axial displacement in terms of the remaining variables, the axial foreshortening effect would be accurately recovered, thus improving the modal representation of the axial displacement field.

Axial displacement analysis for a single mixed element

For the case of a single element, the first step in computing the axial displacement involves substituting the finite-element discretization for u in equation (22). Then, rearranging terms gives:

$$\left(\int_0^l [H_{V_x}]^T [H_{u'}] dx\right)\{q_{u'}\} = \int_0^l [H_{V_x}]^T \left(\frac{V_x}{EA} - \frac{1}{2}w'^2\right) dx \tag{24}$$

The Babuska-Brezzi convergence conditions for mixed elements (see Ref. 18) dictate that:

$$N_u - 1 = N_{V_x} \tag{25}$$

and recalling that $\{q_{u'}\}$ is of length $N_u - 1$, it may be concluded that the coefficient of $\{q_{u'}\}$ in equation (24) is a square matrix. Since that matrix should also be nonsingular in a properly formulated element, equation (24) can be solved for $\{q_{u'}\}$ as follows:

$$\{q_{u'}\} = \left(\int_0^l [H_{V_x}]^T [H_{u'}] dx\right)^{-1} \int_0^l [H_{V_x}]^T \left(\frac{V_x}{EA} - \frac{1}{2}w'^2\right) dx \tag{26}$$

Thus, equation (26) accomplishes the goal of using the mixed finite-element equations to express the axial displacement *explicitly* in terms of the foreshortening effect. And since $u_e = \frac{V_x}{EA}$, equation (26) formally reveals the links between the mixed finite-element, the axial elongation variable, and the axial force variable methods.

Axial displacement analysis for structures of arbitrary geometry: extensibie-inextensible decomposition of the displacement field

If the axial force equations (i.e., the $\{\delta q_{V_x}\}$ equations) of *all* the elements of an arbitrary structural model are collected together, they can be written in the form:

$$[\bar{U}]\{q_u\} = -[\bar{V}]\{q_{V_x}\} + \{f_{FS}\} \tag{27}$$

where $[\bar{U}]$ ($N_V \times N_U$) and $[\bar{V}]$ ($N_V \times N_V$) are matrices and $\{f_{FS}\}$ ($N_V \times 1$) are the nonlinear terms arising from axial foreshortening, in which N_V is the number of force degrees of freedom, and N_U is the number of displacement degrees of freedom. Since the model is assumed to contain only structural elements, $N = N_U + N_V$ where N is the total number of degrees of freedom.

Before proceeding to solve for the axial displacements, it is helpful to examine the axial force equations to gain insights into the properties of the displacement field. Key features of the displacement field can be discerned from the structure of the matrix $[\bar{U}]$. It is well-known from basic matrix theory (see Ref. 19) that for a given matrix $[\bar{U}]$, the basis of the space of vectors of dimension N_U can be partitioned into two orthogonal subsets. Each vector in the first subset has the property $[\bar{U}]\{q\} = 0$, and the dimension of this subset is $nullity(\bar{U})$. The subspace spanned by this subset, usually termed the *null space*, does not generate axial forces in the linear model equations, so the null space may be referred to as the *inextensible subspace*. Each vector in the second basis vector subset has the property $[\bar{U}]\{q\} \neq 0$, and the subspace spanned by this sub-basis may be referred to as the *extensible subspace*. The dimension of the extensible subspace is $rank(\bar{U})$. The dimensions of the two subspaces satisfy:

$$rank(\bar{U}) + nullity(\bar{U}) = N_U \tag{28}$$

which means that the combined basis vector set is complete and that any displacement vector may be regarded as a linear combination of the extensible and inextensible basis vectors. The measure numbers of the extensible and inextensible bases are, respectively, the extensible and extensible coordinates of a vector, and may be viewed as generalizations of the axial and non-axial degrees of freedom of the single element structural model.

Another important result from basic matrix theory is that

$$dimension(range(\bar{U})) = rank(\bar{U}) \tag{29}$$

which implies that if $rank(\bar{U}) < N_V$, then not all the axial force degrees of freedom are linearly independent. The model then has redundant or multiple load paths, and the degree of redundancy is equal to the number of independent relationships among the axial force degrees of freedom. These relationships are generated from the solution process to be described shortly.

Solution of the axial force equations

Solving the axial force equations for the extensible coordinates in terms of the axial force and foreshortening terms allows the extensible coordinates to be eliminated from the system equations, and is analogous to the procedure used earlier to eliminate the Lagrangian axial displacements from the equations for a single blade element.

The extensible coordinates may be obtained with the aid of the *singular-value decomposition* of $[\bar{U}]$:

$$\left[\bar{U}\right] = [A]\,[\Sigma]\,[B]^T \tag{30}$$

where $[A]$ ($N_V \times N_V$) are the left singular vectors, and B^T ($N_U \times N_U$) are the right singular vectors. The matrix $[\Sigma]$ may be written as:

$$[\Sigma] = [\,\Sigma_T \quad 0\,] \tag{31}$$

where $[\Sigma_T]$ is a diagonal matrix that lists, in descending order, the positive square roots of the eigenvalues of $\left[\bar{U}\right]\,\left[\bar{U}\right]^T$. Since $\left[\bar{U}\right]\,\left[\bar{U}\right]^T$ is generally positive semi-definite, its eigenvalues are either zero or positive. The positive eigenvalues correspond to the extensible displacement field, and will be denoted with the subscript ext, while the zero eigenvalues are associated with the inextensible displacement field, and will be denoted with the subscript $inext$. It proves convenient to write $[\Sigma]$ as:

$$[\Sigma] = \begin{bmatrix} \Sigma_{ext} & 0 \\ 0 & 0 \end{bmatrix} \tag{32}$$

where $[\Sigma_{ext}]$ ($rank(\bar{U}) \times rank(\bar{U})$) contains the positive part of $[\Sigma_T]$. The matrices $[A]$ and $[B]$ are orthogonal matrices, in which the columns of $[A]$ are the eigenvectors of $\left[\bar{U}\right]\,\left[\bar{U}\right]^T$, and the columns of $[B]$ are the eigenvectors of $[\bar{U}]^T[\bar{U}]$. It follows that $[A]$ and $[B]$ may be partitioned as follows:

$$[A] = [A_{ext}|A_{inext}] \tag{33}$$

$$[B] = [B_{ext}|B_{inext}] \tag{34}$$

The ordering of the columns of $[A]$ and $[B]$ pertaining to nonzero eigenvalues matches the ordering of their corresponding eigenvalues in $[\Sigma]$.

Since the columns of $[B]$ span the finite-element space, an arbitrary vector $\{q_u\}$ may be expanded as follows:

$$\{q_u\} = [B] \left\{ \begin{array}{c} q_{ext} \\ q_{inext} \end{array} \right\} \tag{35}$$

Substituting equation (35) into equation (27), premultiplying by $[A]^T$, and then premultiplying the top partition by $[\Sigma_{ext}]^{-1}$ gives:

$$\{q_{ext}\} = [\Sigma_{ext}]^{-1}\,[A_{ext}]^T\left(-[\bar{V}]\{q_V\} + \{f_{FS}\}\right) \tag{36}$$

$$0 = [A_{inext}]^T\left(-[\bar{V}]\{q_V\} + \{f_{FS}\}\right) \tag{37}$$

The total displacement field is obtained by adding the foreshortening displacements to the linear and steady-state displacements (see equation 8):

$$\{q_u\} = \{q_{ss}\} + [\Phi]\{q_{modal}\} + \{q_{foreshortening}\} \tag{38}$$

where:

$$\{q_{foreshortening}\} \quad = \quad [B_{ext}](\Sigma_{ext})^{-1}[A_{ext}]^T\{f_{FS}\} \tag{39}$$

in which the contribution of the axial forces to the displacement field, $[\Sigma_{ext}]^{-1}[A_{ext}]^T\left(-[\bar{V}]\{q_V\}\right)$, has been absorbed into $[\Phi]\{q_{modal}\}$. Strictly speaking, $\{q_{ss}\}$ should be computed only from the linear blade equations so that the axial foreshortening generated by the static response will not get computed twice.

Equation (36) is a generalization to models of arbitrary geometry of the axial displacement equation derived earlier for a single element (see equation 26). Equation (37) is the equation mentioned earlier that relates axial force degrees of freedom when the model is redundant. Note that in redundant structures, the extensible displacement field may produce nonzero foreshortening in elements belonging to the multiple load paths, and this will result in $\{q_{ext}\}$ being present on both sides of equation (36). However, if the elements are quite stiff in the axial direction, as they generally are in rotorcraft blades, the foreshortening caused by the extensible displacements will be small in comparison with the foreshortening caused by the inextensible displacements, and will be readily accounted for during the solution iterations.

Applicability of the method

The method sits atop the general finite-element procedure described earlier and therefore, there are no limitations whatsoever on the model's geometry. The geometry restrictions that are often introduced into the axial force variable method (see, for example, Ref. 6) to permit the axial displacements to be computed explicitly, have not been introduced here.

The method was formally derived from equation (27), which was in turn obtained from the mixed finite-element equations for beam axial force degrees of freedom. Thus, the most obvious application of the method is to assemblages of beam components, and it is expected that a common application of the method will be the analysis of redundant, rotorcraft blade models composed of beams. However, there already are several methods available that can analyze the behavior of such models, and it is important to realize that the value of the method presented here is that it is potentially applicable to a far broader range of structural models. To understand why this is so, note that equation (27), from which the method is obtained, is simply a discretized form of the relationship between axial force and axial strain degrees of freedom in beams. But the peculiar form of equation (27) is a consequence of the structure of the nonlinear axial strain tensor, and equations having similar forms will appear in *all* structural components in which axial strains arise, and not just in beams. Therefore, the method, which follows from equation (27), should apply just as broadly. For example, Ref. 14 shows how the method may be applied to the analysis of laminated composite plates employing von Karman plate kinematics. Studies are ongoing that seek to apply and validate the method for complex, higher-order finite-element models of rotor blades containing two-dimensional structural components as well as beams.

Conclusions

The analysis issues associated with several blade formulations have been examined by applying them to the Hodges-Dowell blade equations, specialized to flap-axial motions. It has been shown that classical displacement-based finite elements, while permitting full topological generality, are problematic owing to the near inextensibility of the blade, which makes the small, but critical, axial strain difficult to approximate accurately in reduced basis analyses. Two solutions to the problem were considered, both of which employ the axial force, or a related quantity, as a variable in the analysis. The first of these replaces the axial displacement with the axial force as a solution variable, and may lead to restrictions on the geometry of the model that can be analyzed. The second approach, the mixed finite-element method, removes these geometry restrictions, but introduces additional degrees of freedom into the analysis. Numerical examples demonstrating the effectiveness of the mixed finite-element method for the eigenanalysis and periodic solution of a rotor blade were presented. It was seen that the axial displacement was approximated less accurately than the flap, lag and torsion displacements. To remedy this problem, a method was proposed that generalizes the

notions of "axial displacement" and "bending displacement" to displacements that cause the blade to extend and not to extend. Then, the mixed finite-element axial force equations are used to eliminate the extensible displacements in favor of inextensible displacement and axial force degrees of freedom. This elimination process reduces the number of degrees of freedom in the analysis, but more importantly, it explicitly embeds the nonlinear axial foreshortening effect in the axial displacement calculation. The analysis was first developed for a single mixed element, and then extended to an arbitrary assemblage of elements. It was shown that the method is potentially applicable to highly intricate finite-element mesh geometries that can include two dimensional and three dimensional finite elements, a feature which distinguishes the method from most others that have been proposed for reduced basis analyses of rotor blades.

Acknowledgments

A key motivation for authors' investigations on applying the mixed finite-element method to rotor blade modal reduction was the excellent study on this subject Ref. 8 led by Professor Olivier A. Bauchau of the Georgia Institute of Technology. The authors are also deeply indebted to Professor Bauchau for the valuable advice and information he gave them during their investigations. The authors also thank Dr. Wayne R. Johnson of the Army/NASA Rotorcraft Division at Ames Research Center for his advice and encouragement.

References

[1] Vigneron, F. R., "Stability of a Freely Spinning Satellite of Crossed-Dipole Configuration," *C.A.S.I. Transactions*, Vol. 3, (1), March, 1970, pp. 8–19.

[2] Vigneron, F. R., Comment on "Mathematical Modeling of Spinning Elastic Bodies for Modal Analysis," *AIAA Journal*, Vol. 13, (1), January, 1975, pp. 126–127.

[3] Kaza, K. R. V., and Kvaternik, R. G., "Nonlinear Flap-Lag-Axial Equations of a Rotating Beam," *AIAA Journal*, Vol. 15, (6), June, 1977, pp. 871–874.

[4] Hodges, D. H., Ormiston, R. A., and Peters, D. A., "On the Nonlinear Deformation Geometry of Euler-Bernoulli Beams," NASA TP-1566, April, 1980.

[5] Kane, T. R., Ryan, R. R., and Banerjee, A. K., "Dynamics of a Cantilever Beam Attached to a Moving Base," *AIAA Journal of Guidance, Control and Dynamics*, Vol. 10, (2), March-April, 1987, pp. 139–151.

[6] Smith, E. C., "Aeroelastic Response and Aeromechanical Stability of Helicopters with Elastically Coupled Composite Rotor Blades," UM-AERO 92-15, July, 1992.

[7] Hodges, D. H., "A Mixed Variational Formulation Based on Exact Intrinsic Equations for Dynamics of Moving Beams," *International Journal of Solids and Structures*, Vol. 20, (11), 1990, pp. 1253–1273.

[8] Bauchau, O. A., and Guernsey, C., "On the Choice of Appropriate Bases for Nonlinear Dynamic Analyses," *Journal of the American Helicopter Society*, Vol. 38, (4), October, 1993, pp. 26–36.

[9] Noor, A. K., and Peters, J. M., "Reduced Basis Technique for Nonlinear Analysis of Structures," *AIAA Journal*, Vol. 18, (4), 1980, pp. 455–462.

[10] Ruzicka, G. C., and Hodges, D. H., "Application of the Mixed Finite Element Method to Rotor Blade Modal Reduction," Eighth ARO Workshop on Aeroelasticity of Rotorcraft Systems, State College, Pennsylvania, October 18-20, 1999.

[11] Ruzicka, G. C., and Hodges, D. H., "Application of the Mixed Finite-Element Method to Rotor Blade Modal Reduction," *Mathematical and Computer Modelling,* Vol. 33, (10)-(11), May-June, 2001, pp. 1177–1202.

[12] Shaw, S. W., and Pierre, C., "Normal Modes for Non-Linear Vibratory Systems," *Journal of Sound and Vibration*, Vol. 164, (1), 1993, pp. 85–124.

[13] Pescheck, E., Pierre, C., and Shaw, S. W., "Accurate Reduced Order Models for a Simple Rotor Blade Model Using Nonlinear Normal Modes," *Mathematical and Computer Modelling*, Vol. 33, (10)-(11), May-June, 2001, pp. 1085–1098.

[14] Ruzicka, G. C., and Hodges, D. H., "A Unified Development of Basis Reduction Methods for Rotor Blades," Paper VIB-21316, ASME 2001 Design Engineering Technical Conference, Pittsburgh, Pennsylvania, September 9-12, 2001.

[15] Hodges, D. H., and Dowell, E. J., "Nonlinear Equations of Motion for the Elastic Bending and Torsion of Twisted Nonuniform Rotor Blades," NASA TN D-7818, December, 1974.

[16] "2GCHAS Theory Manual," USAATCOM Technical Memorandum 93-A-004, 1993.

[17] Hodges, D. H.,"Orthogonal Polynomials as Variable-Order Finite Element Shape Functions," *AIAA Journal,* Vol. 21, (5), May, 1983, pp. 796–797.

[18] Szabo, B. A., and Babuska, I., Finite Element Analysis, John Wiley & Sons, 1991.

[19] Golub, G. H., and Van Loan, C. F., Matrix Computations, The Johns Hopkins University Press, 1996.

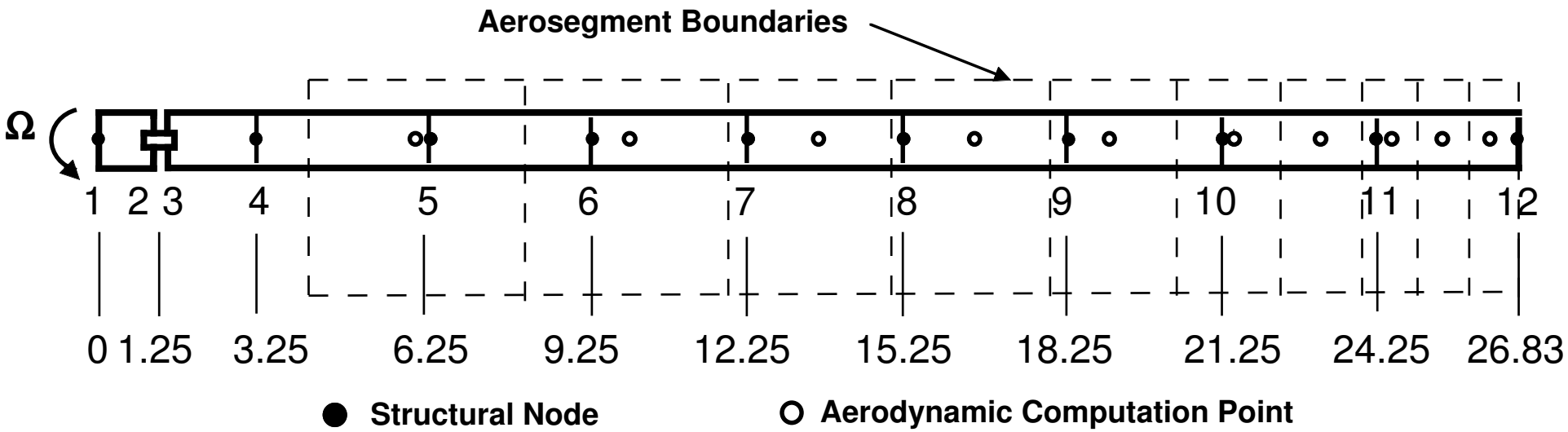

Structural Properties	Aerodynamic Properties	Flight Conditions
Radius - 26.83 ft. EI_y - 1.85E5 lb-ft^2 EI_z - 4.18E5 lb-ft^2 GJ - 2.08E5 lb-ft^2 EA - 6.69E8 lb 92 DOF's	SC1095 Airfoil Uniform Inflow Greenberg Aerodynamics Chord - 1.7405 ft	Ω=258 rev/minute θ_O=10.0 deg. θ_C=2.0 deg. θ_S=-7.0 deg. Θ=4.0 deg. Ψ=Φ=0.0 deg. μ=.373, C_T/σ=.072

Figure 1

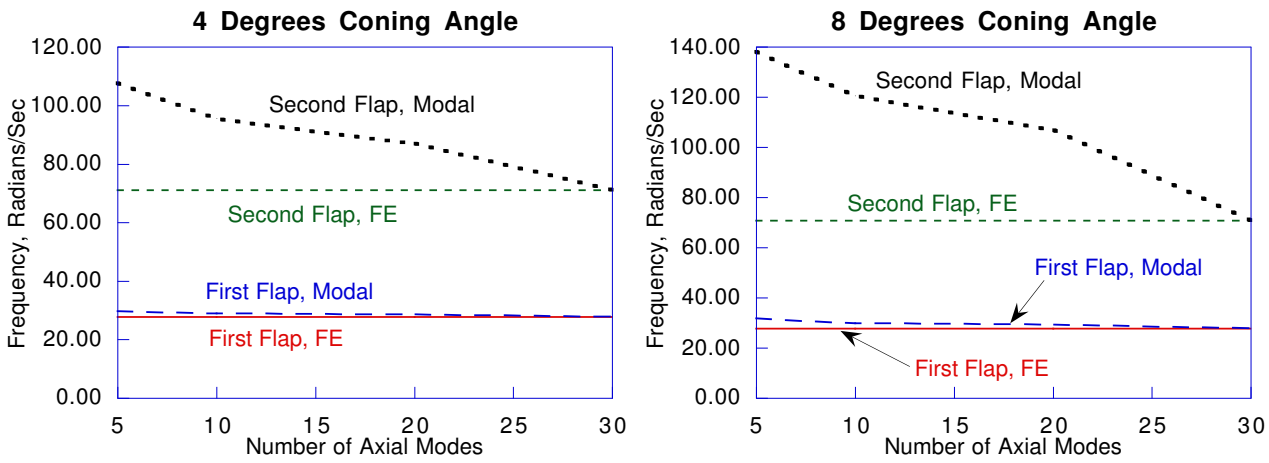
4 Degrees Coning Angle
120.00
100.00
80.00
60.00
40.00
20.00
0.00
Frequency, Radians/Sec
Second Flap, Modal
Second Flap, FE
First Flap, Modal
First Flap, FE
5
10
15
20
25
30
Number of Axial Modes
8 Degrees Coning Angle
140.00
120.00
100.00
80.00
60.00
40.00
20.00
0.00
Frequency, Radians/Sec
Second Flap, Modal
Second Flap, FE
First Flap, Modal
First Flap, FE
5
10
15
20
25
30
Number of Axial Modes

Figure 2

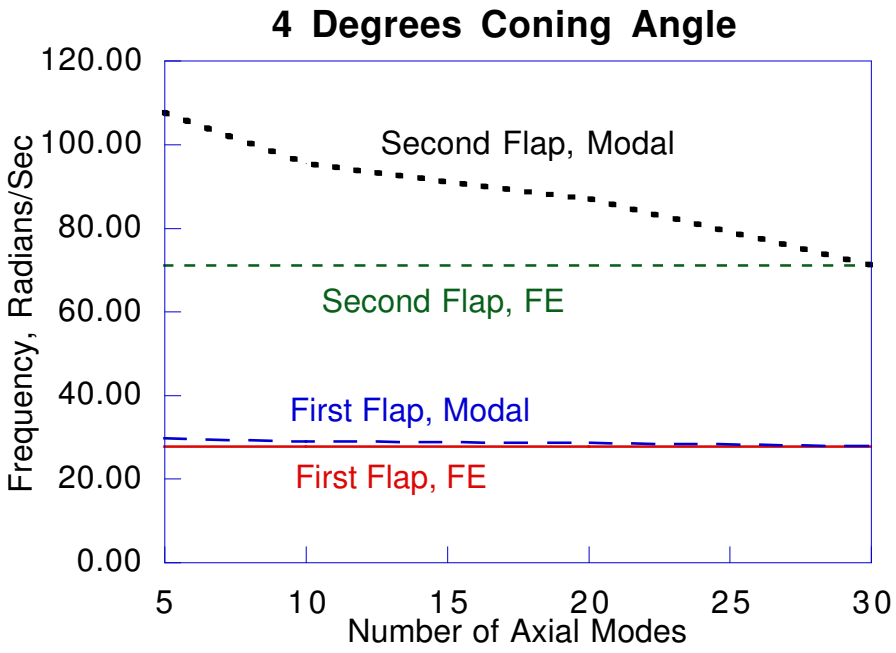
4 Degrees Coning Angle
120.00
100.00
80.00
60.00
40.00
20.00
0.00
Frequency, Radians/Sec
Second Flap, Modal
Second Flap, FE
First Flap, Modal
First Flap, FE
5
10
15
20
25
30
Number of Axial Modes

Figure 2a

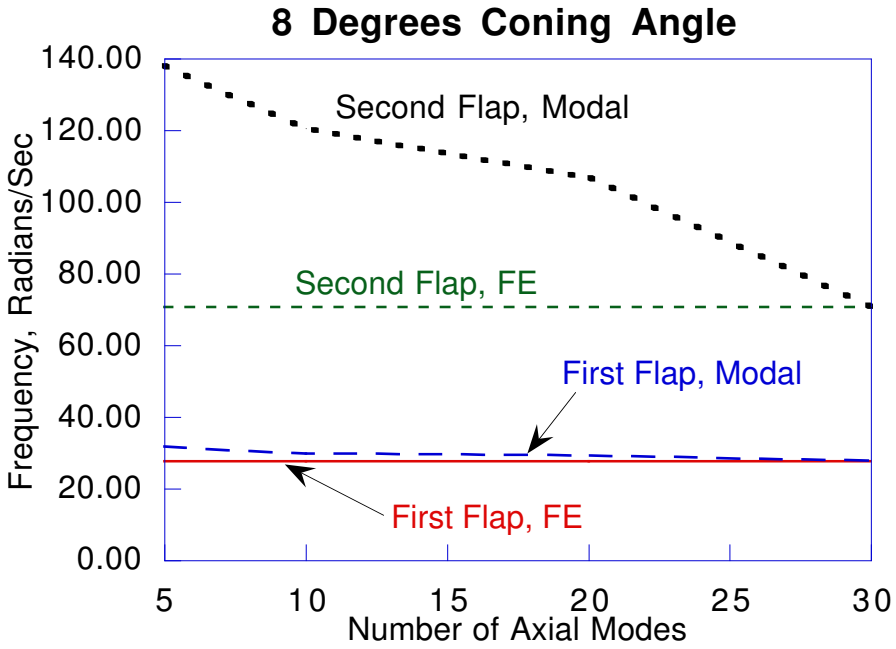
8 Degrees Coning Angle
140.00
120.00
100.00
80.00
60.00
40.00
20.00
0.00
Frequency, Radians/Sec
Second Flap, Modal
Second Flap, FE
First Flap, Modal
First Flap, FE
5
10
15
20
25
30
Number of Axial Modes

Figure 2b

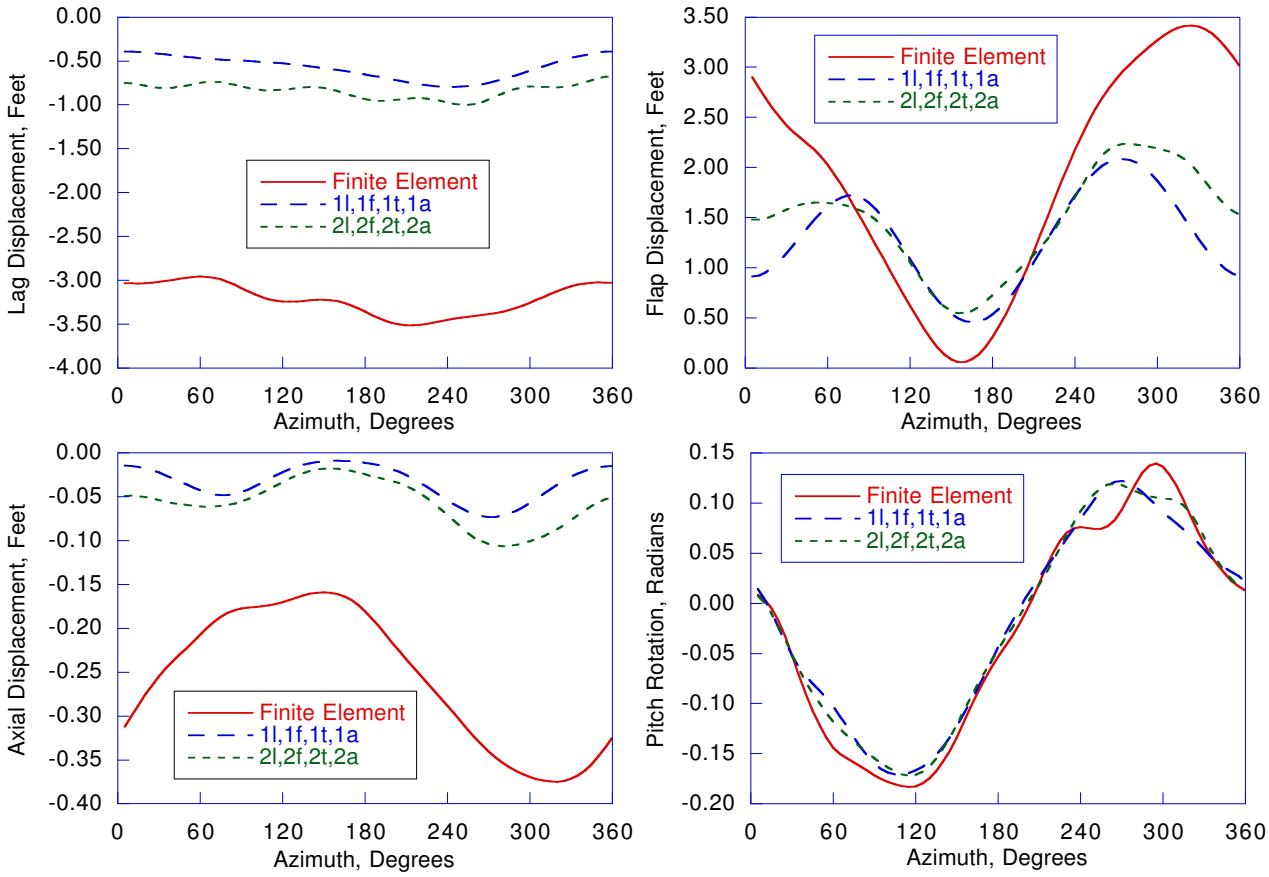
Lag Displacement, Feet
0.00
-0.50
-1.00
-1.50
-2.00
-2.50
-3.00
-3.50
-4.00
Finite Element
1l,1f,1t,1a
2l,2f,2t,2a
0
60
120
180
240
300
360
Azimuth, Degrees
Flap Displacement, Feet
3.50
3.00
2.50
2.00
1.50
1.00
0.50
0.00
Finite Element
1l,1f,1t,1a
2l,2f,2t,2a
Azimuth, Degrees
Axial Displacement, Feet
0.00
-0.05
-0.10
-0.15
-0.20
-0.25
-0.30
-0.35
-0.40
Finite Element
1l,1f,1t,1a
2l,2f,2t,2a
Azimuth, Degrees
Pitch Rotation, Radians
0.15
0.10
0.05
0.00
-0.05
-0.10
-0.15
-0.20
Finite Element
1l,1f,1t,1a
2l,2f,2t,2a
Azimuth, Degrees

Figure 3

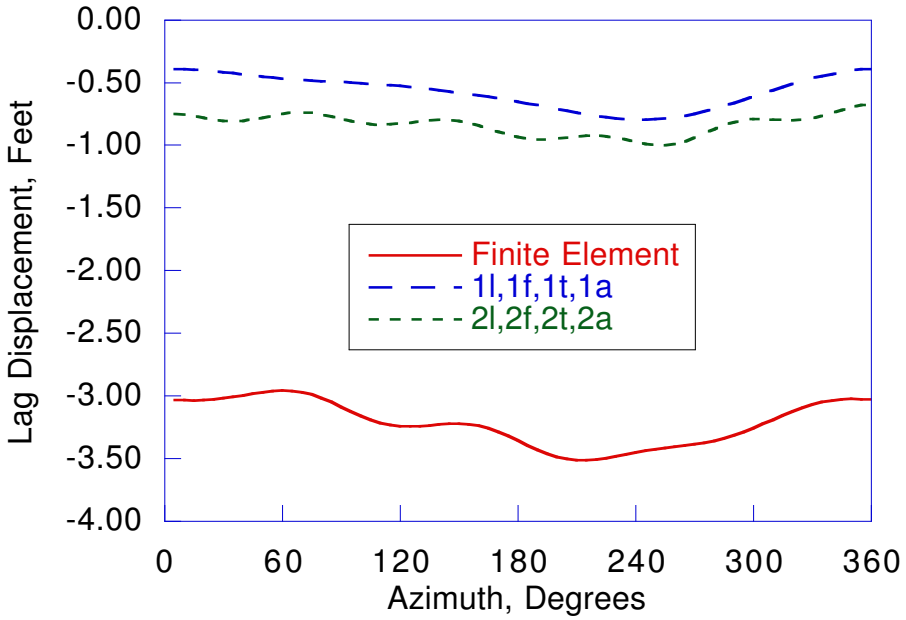
0.00
-0.50
-1.00
-1.50
-2.00
-2.50
-3.00
-3.50
-4.00
Lag Displacement, Feet
0
60
120
180
240
300
360
Azimuth, Degrees
Finite Element
1l,1f,1t,1a
2l,2f,2t,2a

Figure 3a

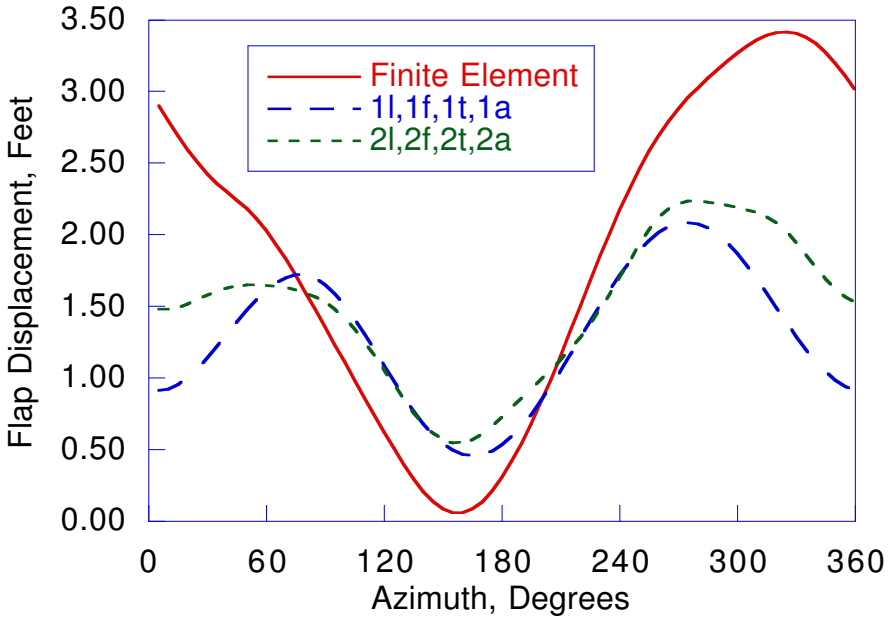
Finite Element
1l,1f,1t,1a
2l,2f,2t,2a
Flap Displacement, Feet
3.50
3.00
2.50
2.00
1.50
1.00
0.50
0.00
0
60
120
180
240
300
360
Azimuth, Degrees

Figure 3b

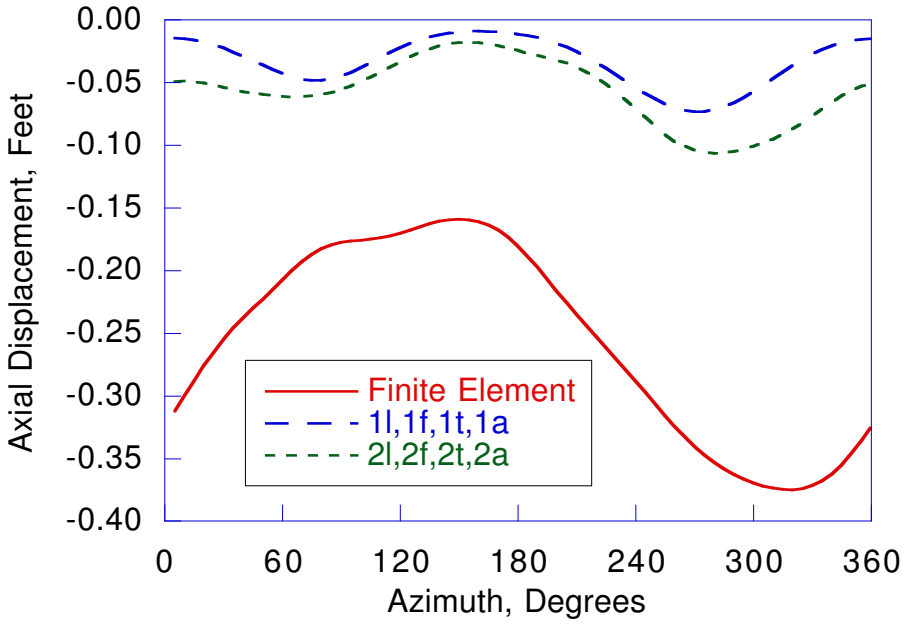
0.00
-0.05
-0.10
-0.15
-0.20
-0.25
-0.30
-0.35
-0.40
Axial Displacement, Feet
0
60
120
180
240
300
360
Azimuth, Degrees
Finite Element
1l,1f,1t,1a
2l,2f,2t,2a

Figure 3c

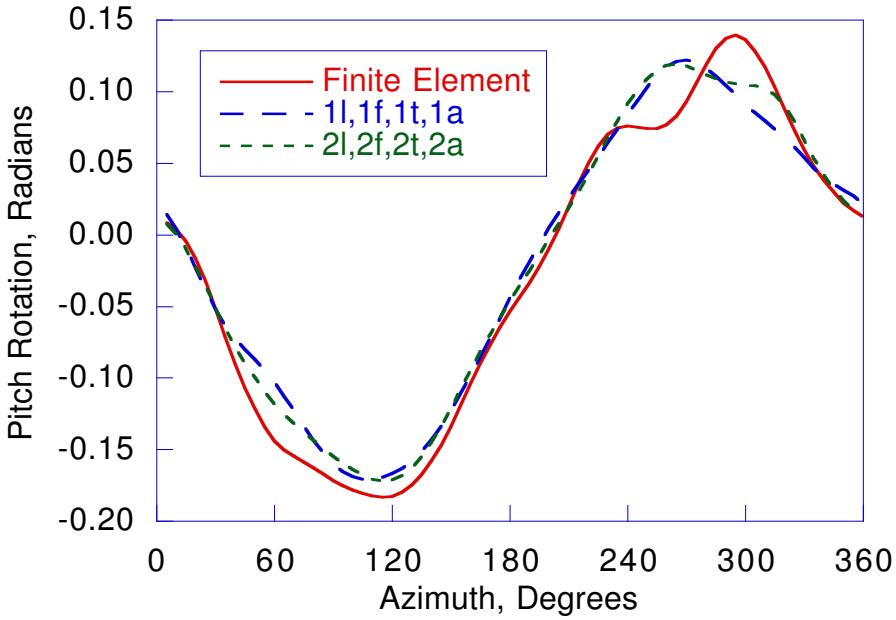
0.15
0.10
0.05
0.00
-0.05
-0.10
-0.15
-0.20
Pitch Rotation, Radians
Finite Element
1l,1f,1t,1a
2l,2f,2t,2a
0
60
120
180
240
300
360
Azimuth, Degrees

Figure 3d

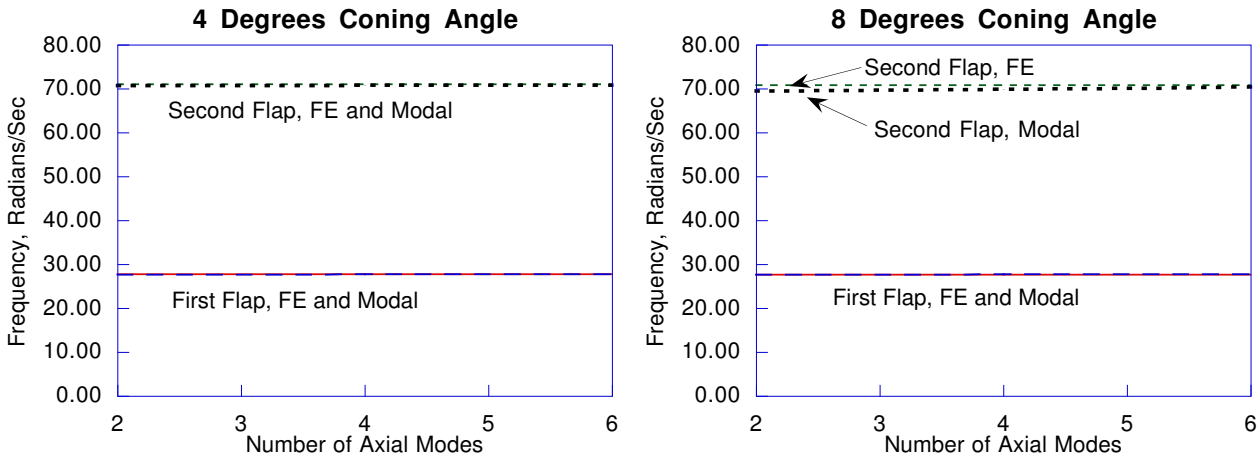
4 Degrees Coning Angle
Frequency, Radians/Sec
80.00
70.00
60.00
50.00
40.00
30.00
20.00
10.00
0.00
Second Flap, FE and Modal
First Flap, FE and Modal
2
3
4
5
6
Number of Axial Modes
8 Degrees Coning Angle
Frequency, Radians/Sec
Second Flap, FE
Second Flap, Modal
First Flap, FE and Modal
Number of Axial Modes

Figure 4

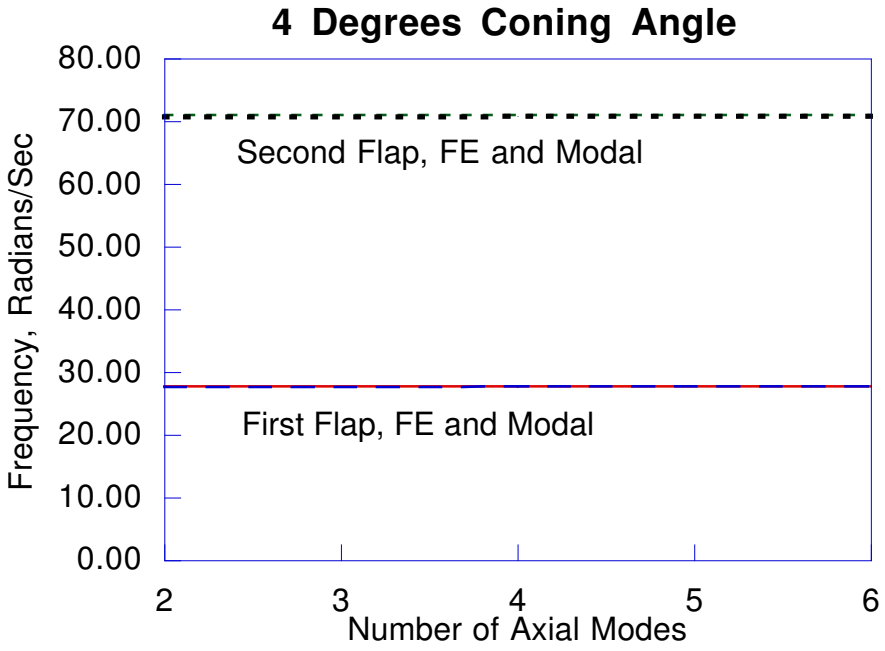
4 Degrees Coning Angle
80.00
70.00
60.00
50.00
40.00
30.00
20.00
10.00
0.00
Frequency, Radians/Sec
Second Flap, FE and Modal
First Flap, FE and Modal
2
3
4
5
6
Number of Axial Modes

Figure 4a

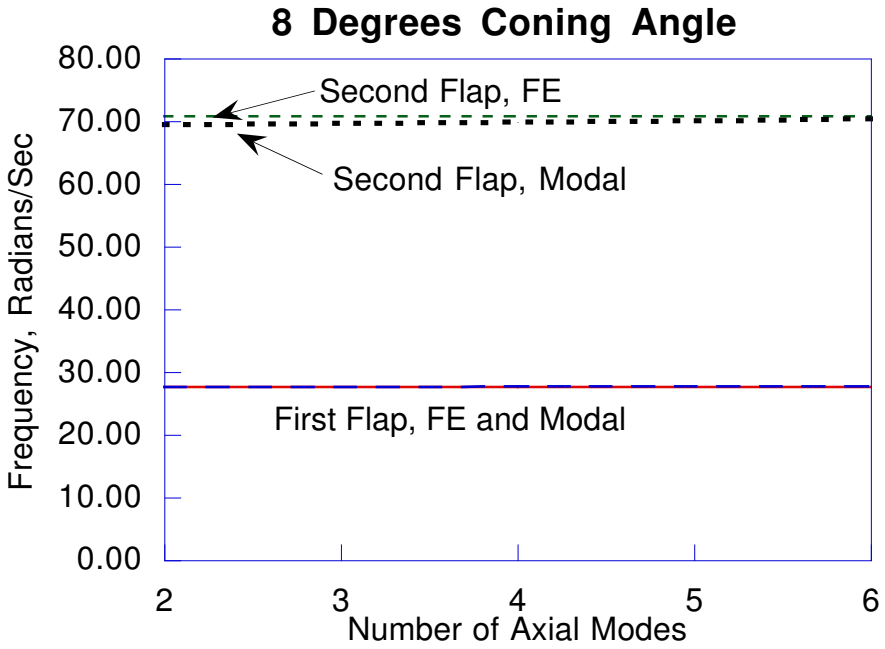
8 Degrees Coning Angle
80.00
70.00
60.00
50.00
40.00
30.00
20.00
10.00
0.00
Frequency, Radians/Sec
Second Flap, FE
Second Flap, Modal
First Flap, FE and Modal
2
3
4
5
6
Number of Axial Modes

Figure 4b

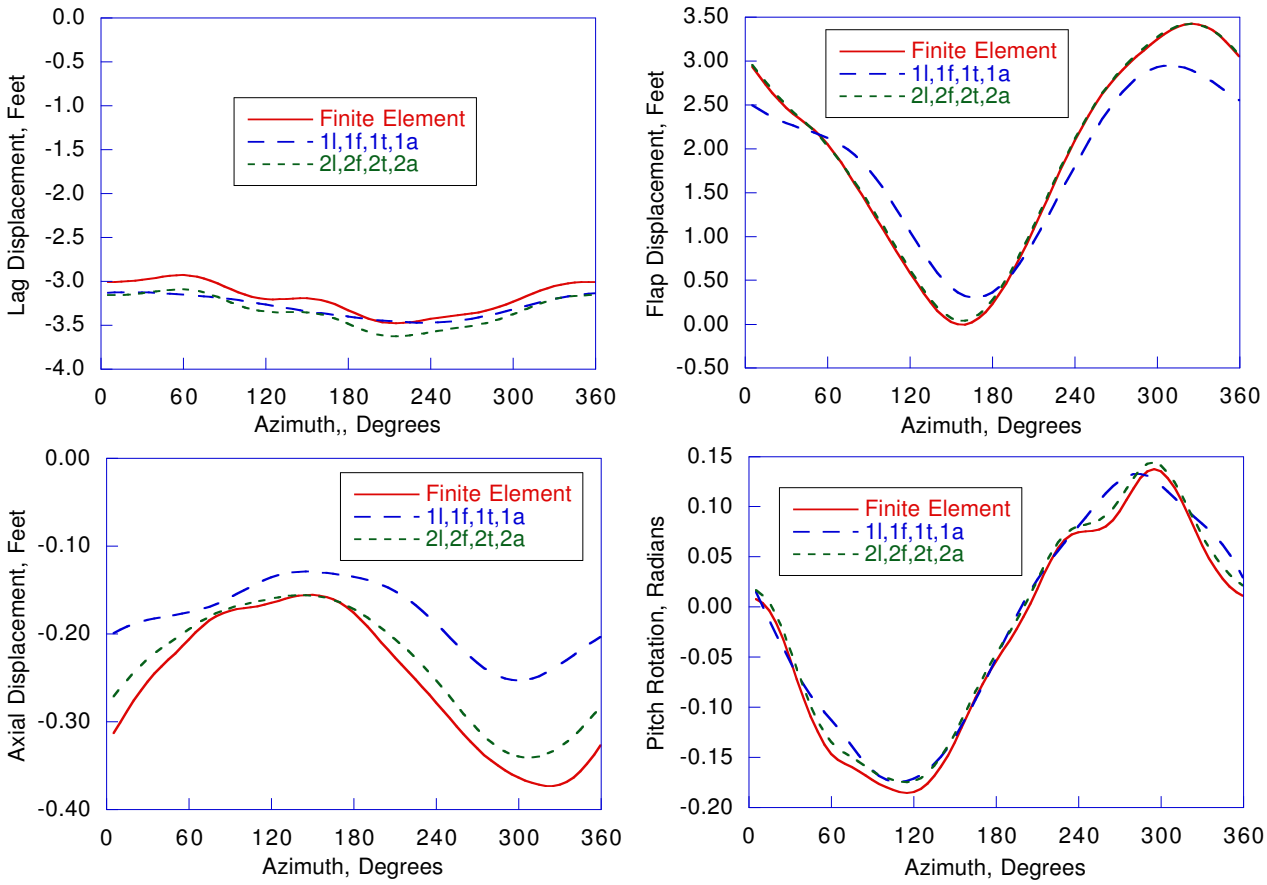
Lag Displacement, Feet
Azimuth,, Degrees
Flap Displacement, Feet
Azimuth, Degrees
Axial Displacement, Feet
Azimuth, Degrees
Pitch Rotation, Radians
Azimuth, Degrees
Finite Element
1l,1f,1t,1a
2l,2f,2t,2a

Figure 5

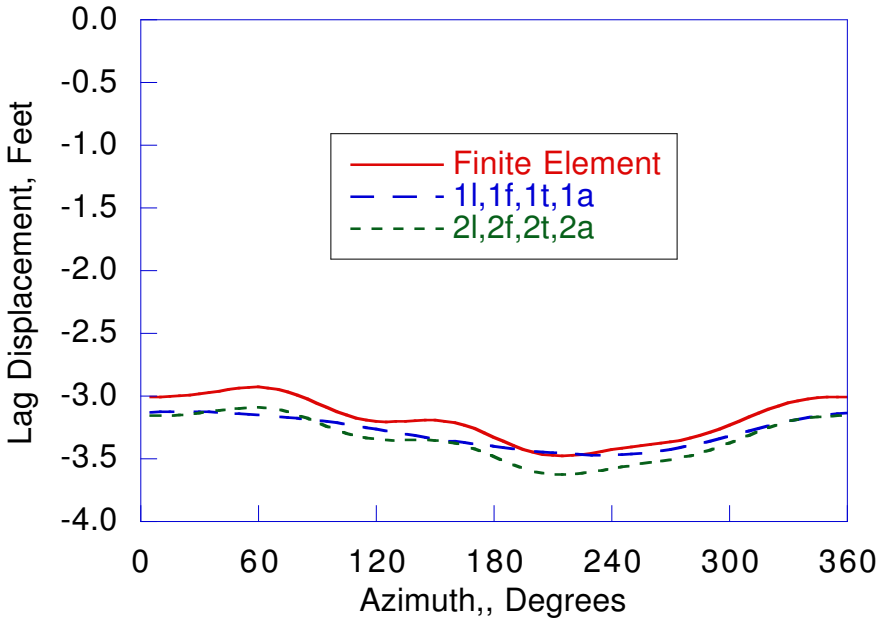
0.0
-0.5
-1.0
-1.5
-2.0
-2.5
-3.0
-3.5
-4.0
Lag Displacement, Feet
Finite Element
1l,1f,1t,1a
2l,2f,2t,2a
0
60
120
180
240
300
360
Azimuth,, Degrees

Figure 5a

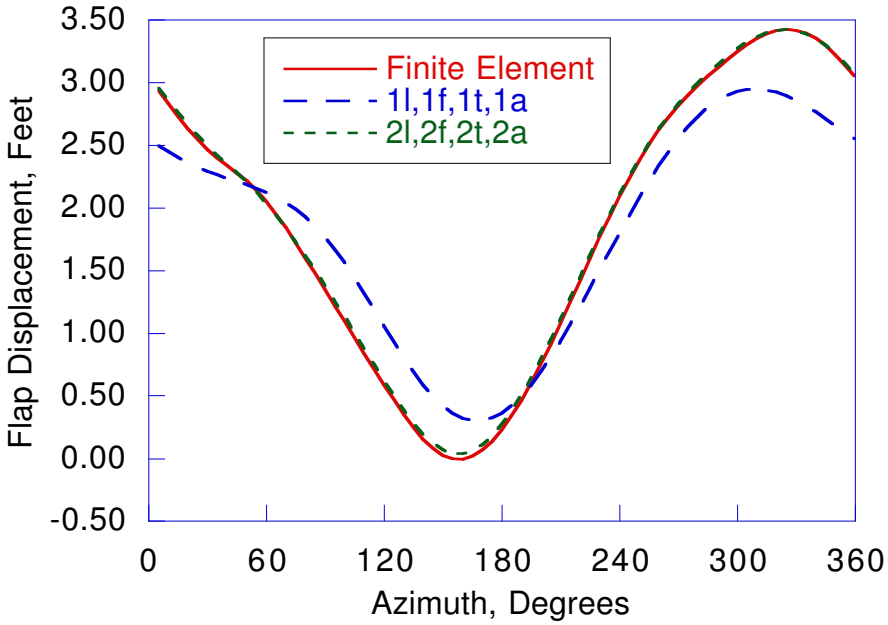
Finite Element
1l,1f,1t,1a
2l,2f,2t,2a
Flap Displacement, Feet
3.50
3.00
2.50
2.00
1.50
1.00
0.50
0.00
-0.50
0
60
120
180
240
300
360
Azimuth, Degrees

Figure 5b

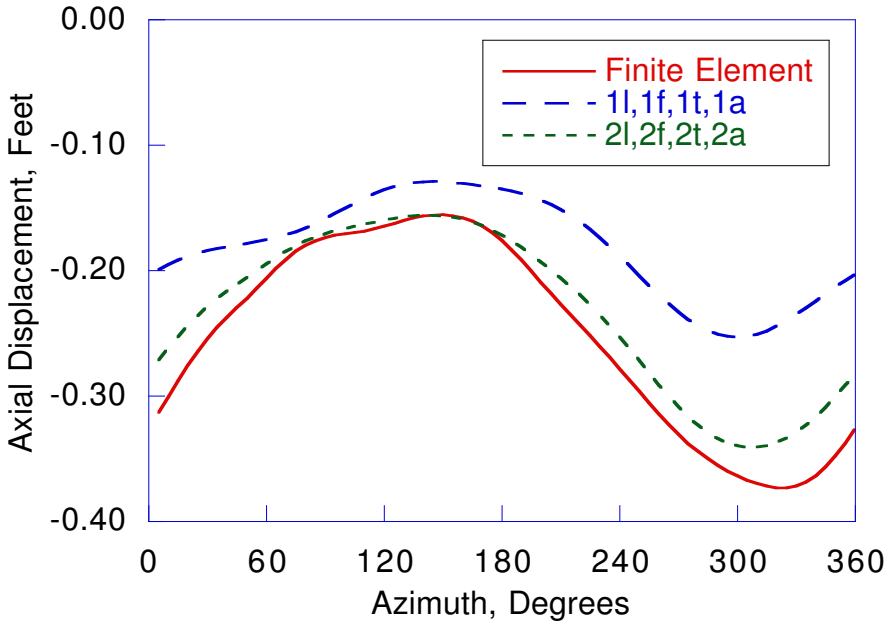
0.00
-0.10
-0.20
-0.30
-0.40
Axial Displacement, Feet
0
60
120
180
240
300
360
Azimuth, Degrees
Finite Element
1l,1f,1t,1a
2l,2f,2t,2a

Figure 5c

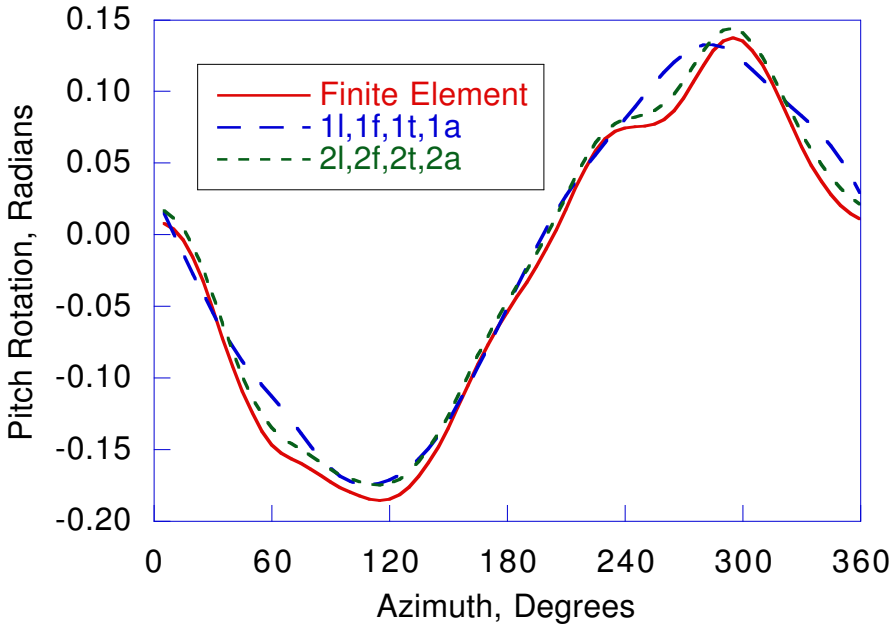
0.15
0.10
0.05
0.00
-0.05
-0.10
-0.15
-0.20
Pitch Rotation, Radians
Finite Element
1l,1f,1t,1a
2l,2f,2t,2a
0
60
120
180
240
300
360
Azimuth, Degrees

Figure 5d

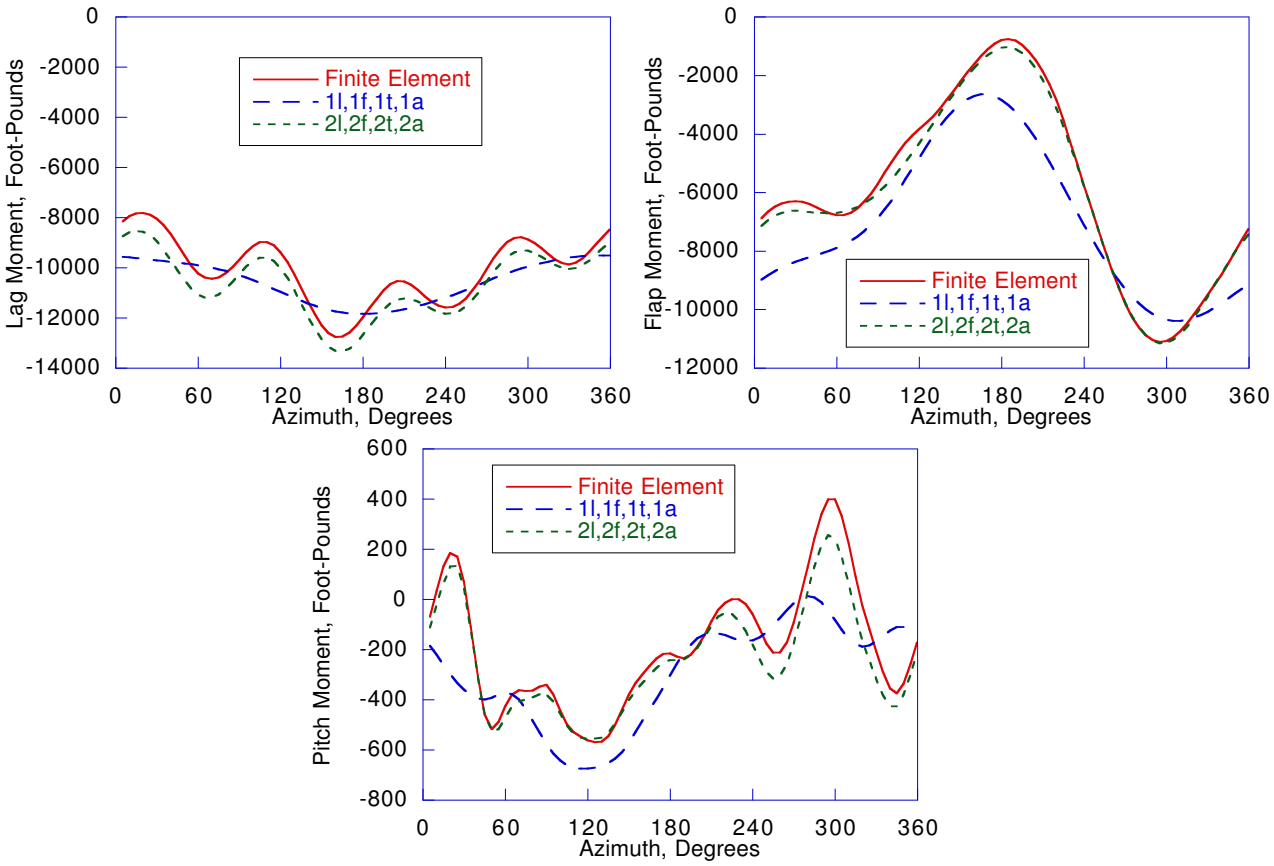
Lag Moment, Foot-Pounds
0
-2000
-4000
-6000
-8000
-10000
-12000
-14000
0
60
120
180
240
300
360
Azimuth, Degrees
Finite Element
1l,1f,1t,1a
2l,2f,2t,2a
Flap Moment, Foot-Pounds
0
-2000
-4000
-6000
-8000
-10000
-12000
0
60
120
180
240
300
360
Azimuth, Degrees
Finite Element
1l,1f,1t,1a
2l,2f,2t,2a
Pitch Moment, Foot-Pounds
600
400
200
0
-200
-400
-600
-800
0
60
120
180
240
300
360
Azimuth, Degrees
Finite Element
1l,1f,1t,1a
2l,2f,2t,2a

Figure 6

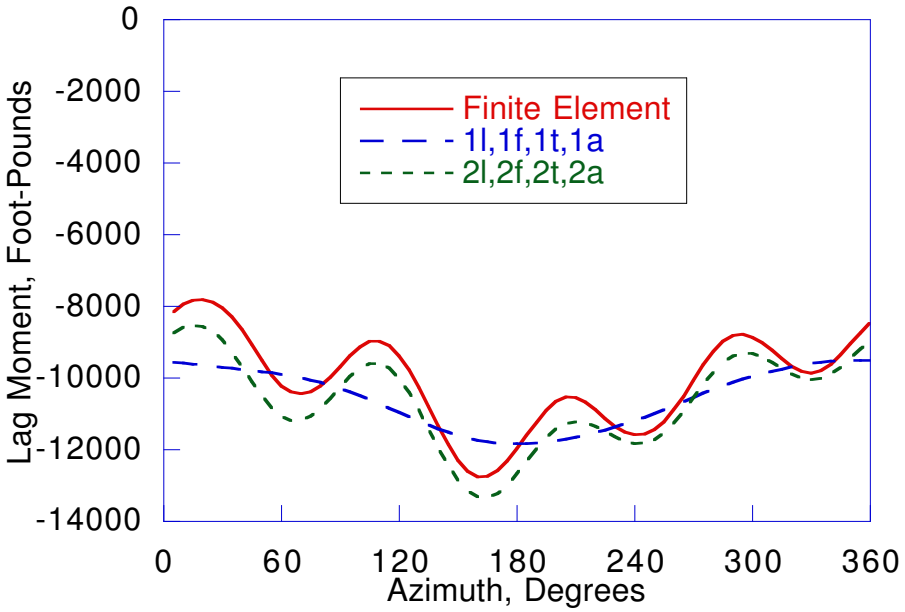
0
-2000
-4000
-6000
-8000
-10000
-12000
-14000
Lag Moment, Foot-Pounds
0
60
120
180
240
300
360
Azimuth, Degrees
Finite Element
1l,1f,1t,1a
2l,2f,2t,2a

Figure 6a

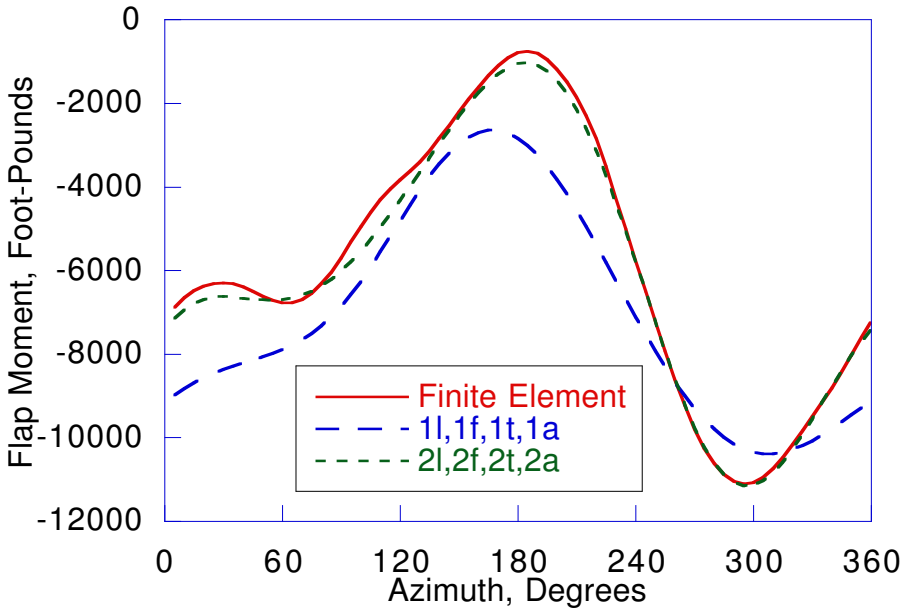
0
-2000
-4000
-6000
-8000
-10000
-12000
Flap Moment, Foot-Pounds
0
60
120
180
240
300
360
Azimuth, Degrees
Finite Element
1l,1f,1t,1a
2l,2f,2t,2a

Figure 6b

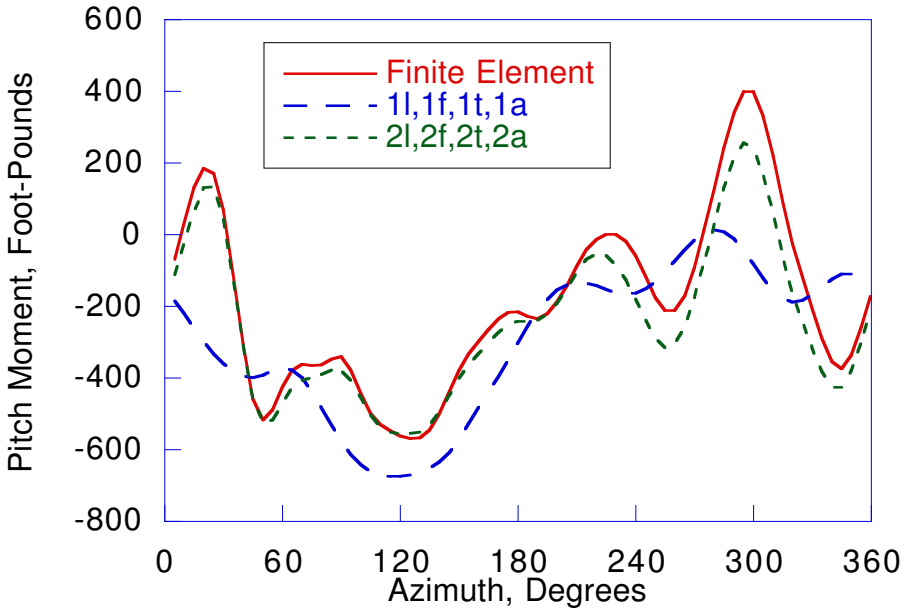
600
400
200
0
-200
-400
-600
-800
Pitch Moment, Foot-Pounds
0
60
120
180
240
300
360
Azimuth, Degrees
Finite Element
1l,1f,1t,1a
2l,2f,2t,2a

Figure 6c

Node	**Displacements**	**Forces**[a]
1	u_1, v_1, v_1', w_1, w_1', ϕ_1	V_{x_1}
2	u_2, v_2, v_2', w_2, w_2', ϕ_2	V_{x_2}
Internal Degrees of Freedom	u_3, u_4, ϕ_3	V_{x_3}

[a]Force degrees of freedom appear only in the mixed element

Table 1

Mode ID	**Frequency (/rev)**
First Lag	0.27
First Flap	1.03
Second Flap	2.63
Second Lag	4.09
First Torsion	4.86
Second Torsion	14.59
First Axial	22.12
Second Axial	66.41

Table 2

Modal Basis	Number of Modes			
	Lag	Flap	Torsion	Axial
1l,1f,1t,1a	1	1	1	1
2l,2f,2t,2a	2	2	2	2

Table 3

Figure Captions

Figure 1: UH-60 blade model.

Figure 2: UH-60 blade flap frequencies: displacement elements.

Figure 3: UH-60 blade tip deflections: displacement elements.

Figure 4: UH-60 blade flap frequencies: mixed Elements.

Figure 5: UH-60 blade tip deflections: mixed elements.

Figure 6: UH-60 blade root loads: mixed elements.

Table Captions

Table 1: Beam finite element degrees of freedom.

Table 2: Articulated blade modes.

Table 3: Description of modal bases.